BJR

https://doi.org/10.1259/bjr.20210598

Received: 13 May 2021 | Revised: 13 January 2022 | Accepted: 20 January 2022 | Published online: 07 February 2022

Cite this article as:
Du Y, Zha H-L, Wang H, Liu X-P, Pan J-Z, Du L-W, et al. Ultrasound-based radiomics nomogram for differentiation of triple-negative breast cancer from fibroadenoma. *Br J Radiol* (2022) 10.1259/bjr.20210598.

FULL PAPER

Ultrasound-based radiomics nomogram for differentiation of triple-negative breast cancer from fibroadenoma

[1]YU DU, MD, [1]HAI-LING ZHA, MD, [1]HUI WANG, MD, [1]XIN-PEI LIU, MD, [1]JIA-ZHEN PAN, MD, [1]LI-WEN DU, MD, [1]MENG-JUN CAI, MD, [2]MIN ZONG, MD, PhD and [1]CUI-YING LI, MD, PhD

[1]Department of Ultrasound, The First Affiliated Hospital of Nanjing Medical University, Nanjing, China
[2]Department of Radiology, The First Affiliated Hospital of Nanjing Medical University, Nanjing, China

Address correspondence to:
Dr Min Zong
E-mail: *mzong@nimu.edu.cn*
Dr Cui-Ying Li
E-mail: *lcy_njmu@163.com*

The authors Yu Du and Hai-Ling Zha contributed equally to the work.

Objective: This study aimed to develop a radiomics nomogram that incorporates radiomics, conventional ultrasound (US) and clinical features in order to differentiate triple-negative breast cancer (TNBC) from fibroadenoma.

Methods: A total of 182 pathology-proven fibroadenomas and 178 pathology-proven TNBCs, which underwent preoperative US examination, were involved and randomly divided into training (n = 253) and validation cohorts (n = 107). The radiomics features were extracted from the regions of interest of all lesions, which were delineated on the basis of preoperative US examination. The least absolute shrinkage and selection operator model and the maximum relevance minimum redundancy algorithm were established for the selection of tumor status-related features and construction of radiomics signature (Rad-score). Then, multivariate logistic regression analyses were utilized to develop a radiomics model by incorporating the radiomics signature and clinical findings. Finally, the usefulness of the combined nomogram was assessed by using the receiver operator characteristic curve, calibration curve, and decision curve analysis (DCA).

Results: The radiomics signature, composed of 12 selected features, achieved good diagnostic performance. The nomogram incorporated with radiomics signature and clinical data showed favorable diagnostic efficacy in the training cohort (AUC 0.986, 95% CI, 0.975–0.997) and validation cohort (AUC 0.977, 95% CI, 0.953–1.000). The radiomics nomogram outperformed the Rad-score and clinical models (p < 0.05). The calibration curve and DCA demonstrated the good clinical utility of the combined radiomics nomogram.

Conclusion: The radiomics signature is a potential predictive indicator for differentiating TNBC and fibroadenoma. The radiomics nomogram associated with Rad-score, US conventional features, and clinical data outperformed the Rad-score and clinical models.

Advances in knowledge: Recent advances in radiomics-based US are increasingly showing potential for improved diagnosis, assessment of therapeutic response and disease prediction in oncology. Rad-score is an independent predictive indicator for differentiating TNBC and fibroadenoma. The radiomics nomogram associated with Rad-score, US conventional features, and clinical data outperformed the Rad-score and clinical models.

INTRODUCTION

Triple-negative breast cancer (TNBC) is regarded as the most aggressive breast cancer, and it is immunohistochemically defined by the negative expression of estrogen receptor, progesterone receptor, and human epidermal growth factor receptor 2.[1] The disease occurs in approximately 10–15% of all breast cancers, and it has a potential correlation with young age and mutation of the TP53 gene and a high degree of correlation with suppressed BRCA1 function.[2] TNBC is a fatal tumor, and it shows less favorable outcomes. In addition, the possible causes of poor outcomes with TNBC include the high pathologic grade and absence of effectively

targeted therapies such as endocrine treatment or trastuzumab.[1,3] The immediate priorities include early detection and personalized treatment.

Conventional breast ultrasonography is an indispensable imaging modality for detection and evaluation of masses in the breast. The predominant ultrasound (US) presentation found that approximately 21–40% of TNBC is oval or round, with a circumscribed margin, parallel orientation, and posterior acoustic enhancement; these morphological characteristics are also typically encountered in fibroadenoma.[3–5] Early studies emphasized that these benign clinical features may impair the diagnostic performance of the US.[3] Although US is a preoperative assessment diagnosing TNBC with non-invasiveness, reproducibility, and no additional cost, the specificity and accuracy should be improved.

Radiomics is an emerging methodology for quantitative analysis of large-scale medical imaging data, and it can automatically filter comprehensive data obtained from an image.[6,7] Recent advances in radiomics-based US are increasingly showing potential for improved diagnosis, assessment of therapeutic response and disease prediction in oncology.[8–12] In previous studies, Luo et al presented that the nomogram incorporating radiomics score and BI-RADS exhibited a potential diagnostic capacity in benign and malignant masses, particularly in BI-RADS categories 4 or 5.[11] Youk et al demonstrated that textural features based on US images had a potential diagnostic performance to distinguish benign and malignant breast cancer.[13] To date, whether radiomics features can differentiate TNBC and fibroadenoma and combined conventional US features and clinical findings can improve the predictive values for distinguishing TNBC from fibroadenoma have not been systematically investigated. Therefore, this study aimed to construct a radiomics nomogram based on conventional US morphological characteristics and clinical findings to differentiate TNBC from fibroadenoma.

METHODS AND MATERIALS

Patients

This retrospective study was approved by the ethics committee of our hospital, and patient consent was waived. Between April 2016 and January 2021, we identified pathology-proven fibroadenomas and pathology-proven TNBCs, which underwent preoperative US examination. The inclusion criteria were as follows: (1) verified lesions after inpatient surgery, (2) complete US and immunohistochemical data, (3) US images acquired from the same ultrasonic instrument, and (4) US images stored by Digital Imaging and Communications in Medicine. The exclusion criteria were as follows: (1) patients who had undergone neoadjuvant chemotherapy, (2) extensive intraductal component, (3) patients receiving biopsy before US examination, and (4) tumor size not fully included in the same plane. Finally, 360 patients involved in our study were randomly separated into training (n = 253) and testing (n = 107) groups. The recruitment flowchart is shown in Figure 1a.

US examination and region-of-interest (ROI) segmentation

The flowchart of radiomics is summarized in Figure 1b, and it can be separated into three parts: imaging acquisition, ROI segmentation, and feature extraction. In addition, the subsequent study flowchart included feature selection, model analysis, and model evaluation. All the US images from the institution were collected using the same US instrument (MyLab Twice, Esaote, Italy) equipped with a 5–13 MHZ linear array transducer. All of the patients were examined in a supine position with full exposure of the breast, including the area closest to the chest wall for good detection of the breast lumps.

In testing the interobserver and intraobserver of the repeatability and reproducibility based on the features extracted from the ROIs, we randomly selected 60 patients for ROI segmentation, and two radiologists with 3 years (Y.D.) and 15 years (H.W.) of experience in breast US scans who were unaware of the pathological results were recruited. The maximal-diameter plane was selected on the basis of the US images of each breast lesion, and then two radiologists drew an ROI along the mass boundary using an open-source application called ITK-SNAP (http://www.itksnap.org). Then, a radiologist (H.W.) repeated the same workflow after 1 month. Features with intraclass correlation coefficients (ICCs) higher than 0.80 in the interobserver and intraobserver agreement extraction were considered for subsequent analysis. The remaining ROI segmentation of the images was accomplished by a radiologist (H.W.).

Clinical information and US conventional features

Clinical characteristics such as age were acquired by reviewing the medical records. US features and the assessment of the BI-RADS category were retrospectively reviewed by two investigators (H.W. and Y.D.), who have 15 and 3 years of experience in breast US examination. Neither of the investigators was involved in the US examination, and both were unaware of the clinical information and pathological data of the patients. They were asked to evaluate and record the imaging features of all the patients. The following image features of breast lesions were recorded and divided into various categories: (1) size (maximum tumor diameter:<3 or>3 cm), (2) shape (oval or round, irregular), (3) margin (well- or non-circumscribed), (4) orientation (parallel or antiparallel), (5) echotexture (hypoechoic or heterogeneous), (6) posterior echo feature (none or enhancement), and (7) BI-RADS category (3, 4A, 4B, 4C, or 5). In cases of discordance, consensus reading was performed, and the consensus data were used for the following analysis.

Radiomics analysis and radiomics construction

Pyradiomics package 2.1.2 was used for the extraction of radiomics features from the ROIs.[14] We used the maximum relevance minimum redundancy (mRMR) algorithm to develop TNBC-related radiomics signatures. The most appropriate feature with non-zero coefficient in the training group among the 360 breast images features was selected using the least absolute shrinkage and selection operator (LASSO) logistic regression algorithm (Figure 2a and b). Then, penalty parameter tuning adjusted by 10-fold cross-validation was used to access the robust and

Figure 1. Workflow of radiomics analysis and study flowchart. (a) Radiomics analysis was divided into three parts: imaging, ROI segmentation, and feature extraction. (b). In the study flowchart, LASSO logistic regression was used to construct radiomics signature and combine with multivariate analysis of the clinical data to develop a nomogram, and then the nomogram was validated in the testing set.

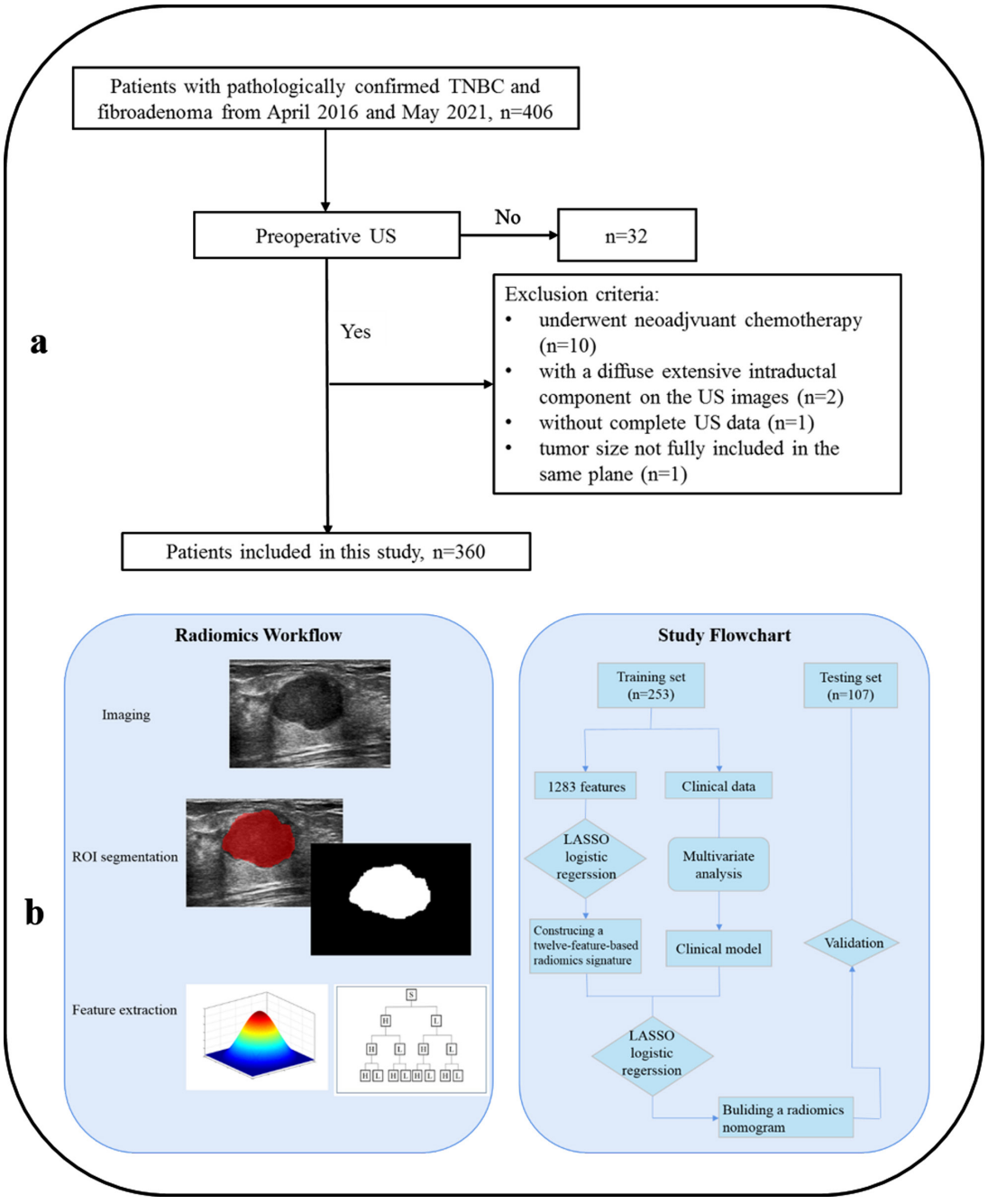

non-redundant features from the initial cohort. Each patient with a Rad-score was created by linear combination of selected features that were weighted by their respective coefficients.[15] The corresponding Rad-score was generated on the basis of the selected features and calculated in all patients in the training and validation groups.

A total of 1283 features were computed and divided into three categories: (1) Nine shape-based features were included for the evaluation of typical morphological features, such as shape and size information about the mass. (2) A total of 216 first-order statistics were considered as first-order parameters, which were used to calculate the distribution of individual voxel intensities through commonly used and basic metrics and ignore the spatial information within the tumors; among the first-order statistics, entropy is consistently considered as a stable feature. (3) A total of 1058 second-order features, generally known as textural features, were included to encode valuable information about

Figure 2. Selection of the radiomics features by using a parametric algorithm was performed in the LASSO binary logistic regression model. (a) Selection of the tuning parameter (λ) was performed in the LASSO model by 10-fold cross-validation based on minimum criteria. A dotted vertical black line was depicted at the optimal value by using the one standard error of the minimum and minimum criteria. The number along the upper axis indicates the average number of predictors. The lower x-axis represents the log(λ), and the y-axis represents binomial deviances. The optimal λ value of 0.040 with log (λ) = −3.688 was selected. (b). LASSO coefficient profiles through the 1283 features. The dotted vertical line was shown at the optimal value using 10-fold cross-validation in A. Features with 12 non-zero coefficients are constructed by using the optimal λ in the plot.

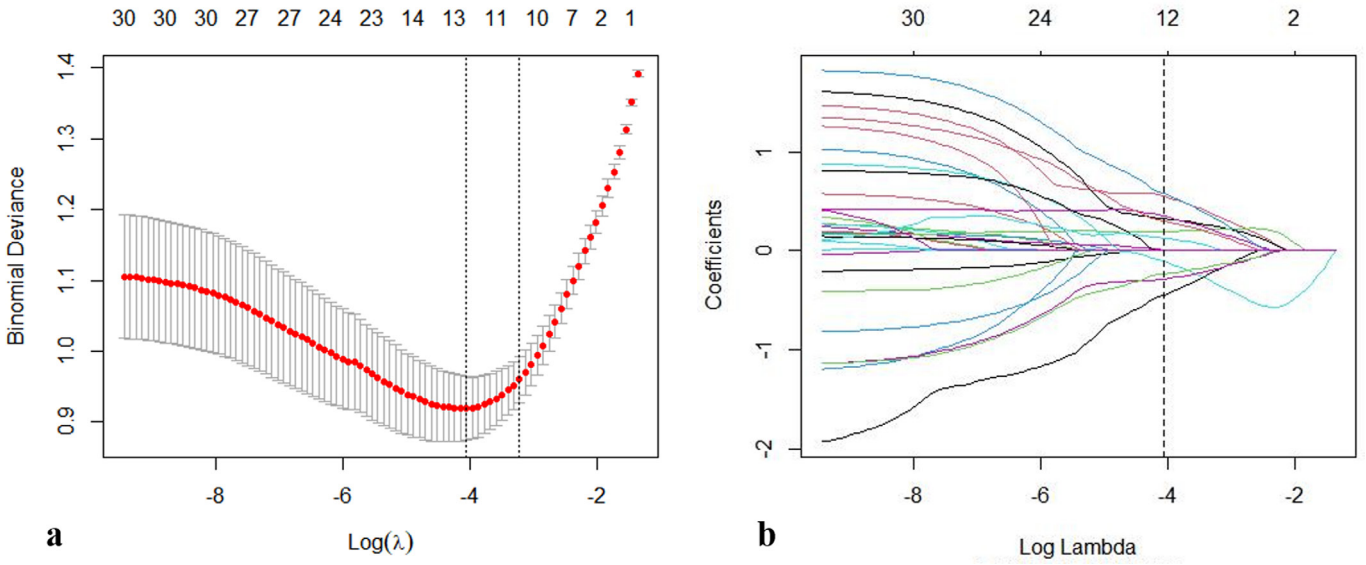

the scene, and such features had a relative spatial arrangement of intensity values in a medical image. In the second-order features, we extracted gray-level co-occurrence matrix (GLCM) features, gray-level dependence matrix (GLDM) features, gray-level size zone matrix (GLSZM) features, gray-level run-length matrix (GLRLM) features, neighboring gray tone difference matrix (NGTDM) features, and wavelet-based features.[16–19]

Establishment and validation of the radiomic nomogram

In this study, the patients were divided into training ($n = 253$) and validation ($n = 107$) datasets using statistical software. One-way analysis of variance was used to compare demographic characteristics and continuous variables as appropriate. The Chi-square test or Fisher's exact test was used to establish significant differences in categorical variables as appropriate. Univariate analyses was used to the screened variables to determine the clinical characteristics that could serve as a potential predictor for TNBC, and variables with $p < 0.1$ were subjected to subsequent analysis. Therewith, a clinical predictive indicator was developed through multivariate logistic regression analysis. Regarding multivariate logistic regression analysis, we applied the variance inflation factor (VIF) to estimate the collinearity diagnostics. The characteristic features were integrated with radiomics signature, and then a radiomics nomogram was developed using multivariate analysis, which provided an individualized and visual model tool for distinguishing TNBC from fibroadenoma.

The potential predictive ability of the established model was assessed by using the receiver operating characteristic (ROC) curve analysis with the area under the curve (AUC). The model performance with a statistical difference of AUC was compared using Delong algorithm ($p < 0.05$). The nomogram model was well-adjusted in accordance with a calibration curve evaluated by the Hosmer–Lemeshow test and used to assess the prediction capability of the nomogram. The discrimination diagnostic performance of the radiomics nomogram model was quantified using the concordance index (C-Index). The range of the C-index was defined as 0.5 to 1.0, with 1.0 corresponding to the best model prediction and 0.5 representing random prediction.[20] Bootstraps with 1000 resamples were calculated for the relatively corrected C-index of the prediction model, and a corrected model was developed. The internal performance of the model was used on all patients in the validation cohort.

Clinical utility of the radiomics nomogram

The discrimination and predictive performance of the established models were assessed on the basis of decision curve analysis (DCA) of the training and validation datasets. DCA was developed to ascertain the clinical utility of the nomogram by quantifying the net benefits at different threshold probabilities in the whole cohort.[21]

Statistical analysis

Statistical analyses were conducted with SPSS (v.26.0) and R statistical software (v.4.0.5)). An independent sample T-test was used to compare continuous data as appropriate. Categorical variables were compared using Fisher's exact test or Chi-square test. LASSO logistic regression analysis was running by "glmnet" package. The "mRMRe" package was applied to implement mRMR algorithm. The VIF values were computed using the "car" package. The ROC curves were plotted using "pROC"

Table 1. Comparisons of clinical and US morphological features in training and validation cohorts

Characteristic	Training cohort (n = 253)	Testing cohort (n = 107)	P
Agea	44.23 ± 13.14	42.71 ± 13.75	0.323
Tumor size			
<3 cm	205 (81.0%)	89 (83.2%)	0.630
>3 cm	48 (19.0%)	18 (16.8%)	
Shape			
Oval or round	128 (50.6%)	56 (52.3%)	0.762
Irregular	125 (49.4%)	51 (47.7%)	
Margin			
Well circumscribed	126 (49.8%)	64 (59.8%)	0.642
Non-circumscribed	127 (50.2%)	43 (40.2%)	
Orientation			
Parallel	213 (84.2%)	88 (82.2%)	0.061
Non-parallel	40 (15.8%)	9 (17.8%)	
Echotexture			
Hypoechoic	198 (78.3%)	91 (85.0%)	0.234
Heterogeneous	55 (21.7%)	16 (15.0%)	
Posterior echo feature			
None	178 (70.4%)	79 (73.8%)	0.505
Enhancement	75 (29.6%)	28 (26.2%)	
BI-RADS category			
3	71 (28.1%)	32 (29.9%)	0.673
4A	66 (26.1%)	26 (24.3%)	
4B	61 (24.1%)	31 (29.0%)	
4C	34 (13.4%)	13 (12.1%)	
5	21 (8.3%)	5 (4.7%)	
Rad-scorea	−0.07 ± 2.06	0.25 ± 1.95	0.160

NOTE: Unless otherwise noted, data are shown as the number of patients, with the percentage in parentheses.
[a]Data are means ± standard deviations.

package. The nomogram and calibration curve were constructed using the "rms" package. The decision curve was plotted using the "dca.r" package. A two-tailed P-value of <0.05 indicated statistical significance.

RESULTS

Clinical characteristics and clinical model

The study flowchart is summarized in Figure 1. Table 1 presents the comparisons of US-based morphology characteristics and clinical data. The training cohort included 54 (50.5%) fibroadenomas and 53 (49.5%) TNBCs, and the validation cohort included 128 (50.6%) fibroadenomas and 125 (49.4%) TNBCs. The results demonstrated no statistical difference between the training and validation cohorts with regard to lesion size, age, and US morphological features (p = 0.061–0.762). Univariate analysis showed that age, tumor size, shape, margin, orientation, posterior echo feature, BI-RADS category, and Rad-score were associated with good statistical significance in the training cohort (Table 2). Based on multivariate analysis, patients' age (odds ratio [OR]: 1.16; 95% CI: 1.09–1.24; $p < 0.001$), a BI-RADS final assessment category of 3 (OR: 0.04; 95% CI: 0.01–1.24; p = 0.001) or 4 (OR of 4B: 7.43; 95% CI: 1.72–32.142; p = 0.007; OR of 4C: 17.84; 95% CI: 2.84–112.23; p = 0.002) or 5 (OR: 23.85; 95% CI: 1.05–539.60; p = 0.001), and Rad-score (OR: 1.06; 95% CI: 1.18–1.32; $p < 0.001$) were considered as independent predictors of the predictive model associated with TNBC. The clinical model was constructed on the basis of age and BI-RADS category, which showed favorable discrimination with an AUC of 0.942 (95%CI: 0.914–0.971) in the training datasets and 0.943 (95% CI: 0.901–0.984) in the testing datasets, respectively.

Features selection and Rad-score building

A total of 1283 radiomics features were selected, and 26 features were extracted by mRMR associated with TNBC. The

Table 2. Results of univariate and multivariate analyses of the potential predictors based on the training cohort

Factors	Univariate analysis OR (95% CI) *P*	Multivariate analysis OR (95% CI) *P*
Age	0.86 (0.82–0.89) <0.001	1.16 (1.09–1.24) <0.001
Tumor size		
<3 cm	1 (ref)	NA
>3 cm	0.58 (0.30–1.10) 0.092	
Shape		
Oval or round	1 (ref)	NA
Irregular	3.51 (2.10–5.90) <0.001	
Margin		
Well circumscribed	1 (ref)	NA
Non-circumscribed	2.34 (1.41–3.87) 0.001	
Orientation		
Parallel	1 (ref)	NA
Non-parallel	2.14 (1.16–4.32) 0.034	
Echotexture		
Hypoechoic	1 (ref)	NA
Heterogeneous	0.73 (0.43–1.26) 0.265	
Posterior echo feature		
None	1 (ref)	NA
Enhancement	2.62 (1.55–4.44) <0.001	
BI-RADS category		
3	0.19 (0.08–0.49) <0.001	0.04 (0.01–1.24) 0.001
4A	1 (ref)	1 (ref)
4B	4.18 (1.99–8.80) <0.001	7.43 (1.72–32.14) 0.007
4C	18.08 (4.99–65.49) <0.001	17.84 (2.84–112.23) 0.002
5	33.00 (4.41–277.38) 0.001	23.85 (1.05–539.60) 0.046
Rad-score	1.26 (1.19–1.37) <0.001	1.16 (1.08–1.32) <0.001

BI-RADS, Breast Imaging Reporting and Data System; CI, confidence interval; OR, odds ratio; TNBC, triple-negative breast cancer; ref, reference.

intraobserver ICCs ranged from 0.824 to 0.988, and the interobserver ICCs ranged from 0.807 to 0.973, indicating satisfactory reproducibility in ROI segmentation. Finally, the features were reduced to 12 potential predictive factors from features with non-zero coefficients using the LASSO regression algorithm (Figure 3). The formula used to calculate by the Rad-score associated with the 12 radiomic features was as follows:

Rad-score = −0.107*exponential_glszm_ZoneEntropy + −0.444*square_glszm_LargeAreaLowGrayLevelEmphasis + 0.551*log-sigma-3–0 mm-2D_firstorder_Skewness + 0.007*squareroot_ngtdm_Coarseness + 0.326*square_ngtdm_Contrast + 0.195*log-sigma-5–0 mm-2D_glcm_Imc1 + −0.284*lbp-2D_glszm_ZoneVariance + 0.35*log-sigma-5–0 mm-2D_glszm_SmallAreaEmphasis + 0.305*log-sigma-5–0 mm-2D_glrlm_ShortRunLowGrayLevelEmphasis + −0.233*gradient_firstorder_Kurtosis + 0.579*wavelet-H_firstorder_Skewness + 0.131*exponential_gldm_DependenceEntropy + −0.071

The Rad-score presented an acceptable diagnostic accuracy in predicting TNBC with an AUC of 0.890 (95% CI: 0.851–0.929) in the training set and 0.886 (95% CI: 0.825–0.948) in the validation set, respectively.

Construction and validation of radiomics nomogram

Clinical and Rad-score models were constructed in accordance with the above-mentioned methods, and both models ascertained the independent predictors of TNBC in the training and testing groups. The radiomics nomogram model incorporated significant clinical morphological predictors with the fusion Rad-score of US images. Among multivariate logistic regression analyses, age, BI-RADS, and Rad-score were identified as potential

Figure 3. Result of feature selection and the verified set of Rad-score. Twelve non-zero coefficients features are presented, including first-order statistics, textural features, and wavelet-based features.

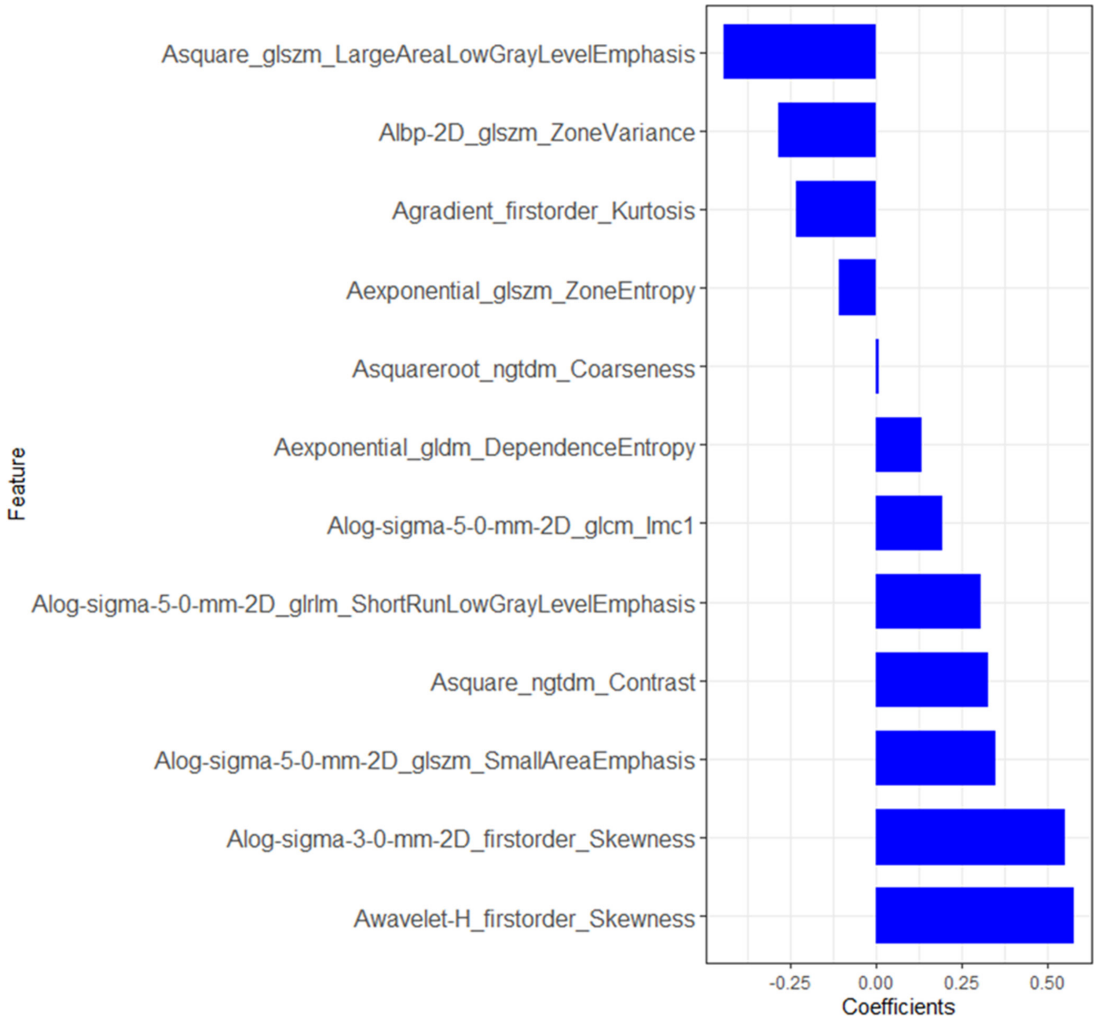

predictors associated with TNBC. The VIF values of the three predictors ranged from 1.13 to 1.19, indicating that no collinearity was found during collinearity diagnosis. A nomogram incorporated with the predictors was established (Figure 4).

The combined model also showed improved diagnostic efficiency in ROC analysis compared with the Rad-score and clinical models (Figure 5a and b). By comparing the models, the combined model presented an optimal performance and the best AUC value (0.986; 95% CI: 0.975–0.997) in the training group. The model also presented the highest AUC (0.977; 95% CI: 0.953–1.000) in the testing cohort. Therefore, we suggested that the nomogram integrated with Rad-score and clinical model for TNBC prediction, with a satisfactory discrimination ability. Figure 5c illustrates the calibration curve of the nomogram in the training cohort, and the Hosmer–Lemeshow test yielded a non-significant statistic (p = 0.732). The calibration curve of the nomogram in the validation cohort and the Hosmer–Lemeshow test showed favorable calibration (Figure 5d) with a non-significant statistic (p = 0.807). The recommended nomogram was integrated with Rad-score and clinical model, with favorable discrimination (C-index, 0.984 in the training cohort and 0.985 in the validation cohort). Hence, our nomogram demonstrated favorable precision in the training and validation cohorts.

In addition, the combined model outperformed the Rad-score model (AUC values of 0.986 *vs* 0.890; $p < 0.001$) and clinical model (AUC values of 0.986 *vs* 0.942; $p < 0.05$) in the training cohort based on the Delong test. In the validation cohort, the combined model also exhibited a better predictive capability than the Rad-score (AUCs of 0.977 *vs* 0.886; $p < 0.001$) and clinical models (AUCs of 0.977 *vs* 0.943; $p < 0.001$).

Clinical usefulness of the nomogram

The decision curves for the clinical model, Rad-score model, and combined nomogram in the training cohort are presented in Figure 6a. The results showed that using the nomogram to predict the risk of TNBC adds more net benefit than the "treat all" or "treat none" strategies and achieves the most net benefit when threshold probabilities ranged from 0.1 to 1.0. Similar results could be found in the testing cohort (Figure 6b).

Figure 4. Combined radiomics nomogram constructed by Rad-score and clinical characteristics for predicting TNBC in the training cohort. The predictors include age, BI-RADS, and Rad-score.

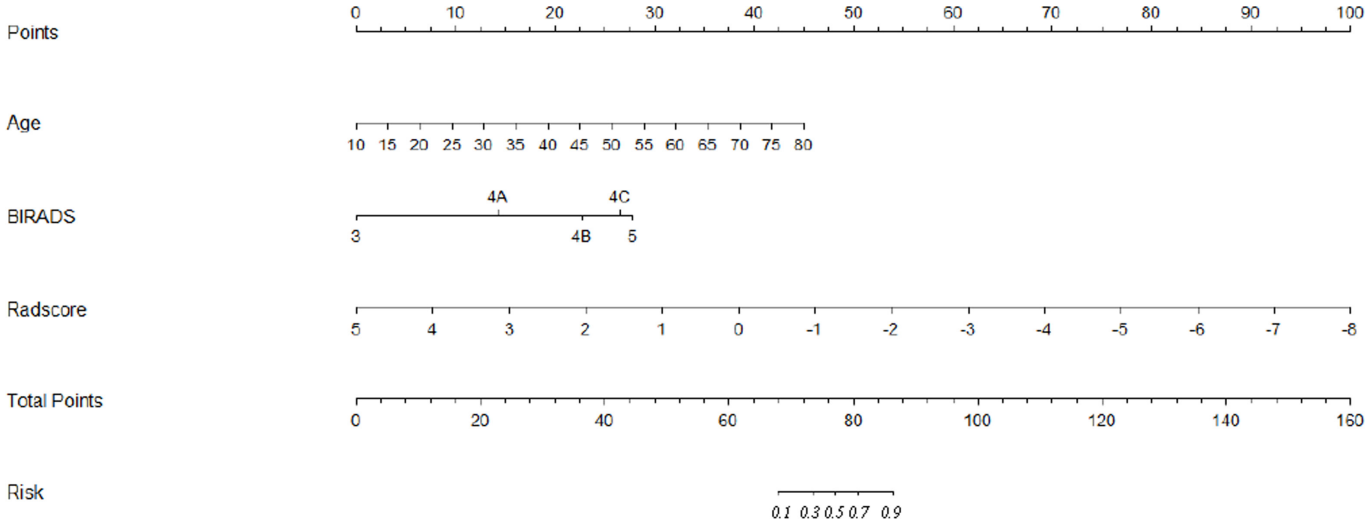

DISCUSSION

In this study, we developed a nomogram-incorporated radiomics signature, US conventional features, and clinical findings to differentiate TNBC from fibroadenoma. The Rad-score not only served as a potential predictive indicator in differentiating TNBC and fibroadenoma but also showed a good performance when combined with the clinical findings.

Radiomics is a computer-aided diagnosis model that uses an automated high-throughput extraction of large amounts of quantitative phenotypic characteristics of medical images and converts features into mathematical models that can provide more and better information than those found by a radiologist.[22–24] The evaluation criteria and reporting guidelines must be completed to develop radiomics analysis and mature discipline.[25] In previous studies, texture analysis demonstrated a favorable performance in the clinical diagnosis based on US morphological features, distinguishing benign and malignant lesions, differentiating breast cancer subtypes, and assessment of therapeutic responses to neoadjuvant chemotherapy, which illustrated the clinical application of radiomics.[9,10,13] Lee et al demonstrated that the Rad-score based on US texture presented a favorable diagnostic performance for differentiating TNBC and fibroadenoma with an AUC of 0.91.[13] In addition, Moon et al designed US-based texture features of computer-aided diagnosis, which can be used to differentiate TNBC from fibroadenoma with an AUC of 0.84. However, 169 patients were involved in this study; thus, the application of this CAD system in every US examination is impossible, and computer feature sets may waste a considerable amount of time when deviating from the multi-resolution gray-scale invariant texture.[26] In our present research, we developed a Rad-score consisting of 12 radiomic features to differentiate TNBC from fibroadenoma, and the Rad-score demonstrated sufficient discrimination performance between the TNBC and fibroadenoma, which further emphasizes the robust capability of radiomics features. Moreover, the Rad-score was in accordance with that of previous studies, and it can serve as a potential indicator for predicting TNBC and fibroadenoma.

In general, US morphological features depend on conventional clinical practices for differentiating variable subtypes of breast cancer. Conventional sonographic features are intuitive, and TNBC has atypical features that are an underestimation of the diagnostic accuracy. Yoon et al presented that TNBC usually showed more suspicious US characteristics with posterior echo enhancement, irregular shape, and a non-circumscribed margin than fibroadenoma.[4] In addition, Yeo et al reported a study predicting TNBC and fibroadenoma based on US alone of 131 patients, showing dissatisfactory results with an AUC of 0.65.[27] This conclusion on TNBCs can be confused with diagnosis because of several distinct sonographic criteria, and it may be associated with benign tumor such as fibroadenoma. In our study, univariate analysis indicated that most US characteristics showed a good diagnostic ability in distinguishing TNBC and fibroadenoma. Multivariate analysis presented that age and BI-RADS category were associated with a predictive clinical model, which can be an effective tool for predicting TNBC and fibroadenoma. Thus, US characteristic is important in constructing a clinical predictive model. However, image acquisition depends on the experience of the radiologist, and different radiologists are skilled in different fields, such as breast, thyroid, and liver. This condition may explain why the AUC of the clinical model was inferior to the radiomics nomogram in this study.

Rapid nomograms are widely used in the response of treatment and prediction of treatment in oncology.[28–30] To our knowledge, this research is the first study that is developed and validated to predict breast lesions with TNBC and fibroadenoma using a radiomics signature-based nomogram. Substantial overlap exists in the conventional US features of TNBC and fibroadenoma. Previous studies have constructed a US-based radiomics signature and proven a radiomics nomogram, which can be used to distinguish benign and malignant lesions and preoperatively predict TNBC.[25,31,32] Luo et al reported a nomogram combined with BI-RADS and radiomics, which showed potential application value for the diagnosis and discrimination of category four or five lesions in BI-RADS.[11] In our study, we constructed and

Figure 5. (a, b)Comparison of the AUCs for the clinical model, Rad-score model, and radiomics nomogram in the training and validation cohorts. (c).Calibration curves of the radiomics nomogram in the training cohort. (d).Calibration curves of the radiomics nomogram in the validation cohort. The X-axis represents the predictive probability; Y-axis denotes the observed probability. The 45° blue diagonal line represents the perfect prediction of TNBC, and the red line indicates the prediction model of the radiomics nomogram. The closer the red line fits to the ideal line, the better the discrimination of the nomogram.

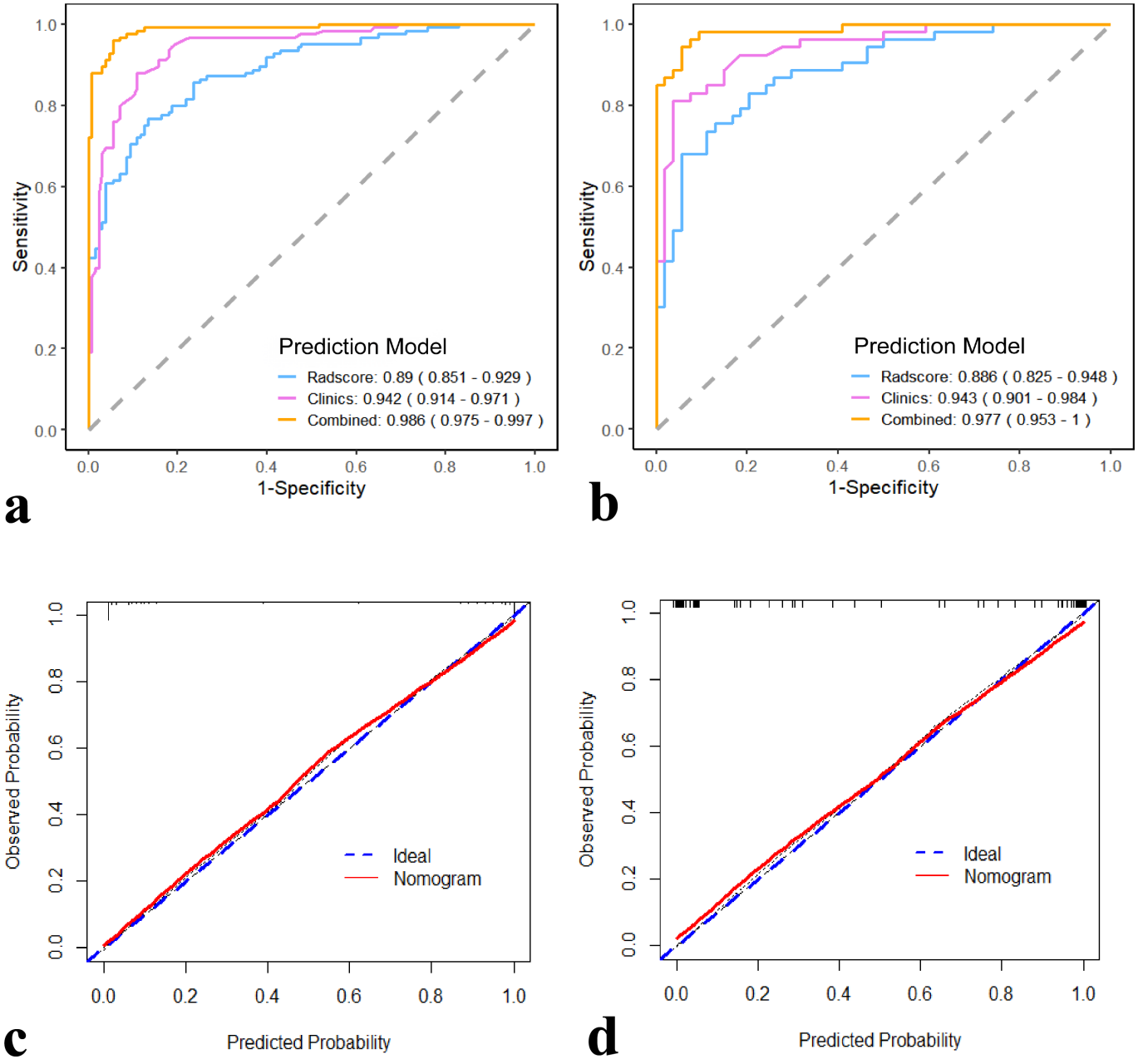

identified radiomics nomogram-incorporated Rad-score and clinical findings to easily distinguish TNBC and fibroadenoma. The nomogram presented an enormous potential for differentiating such lesions with a satisfactory C-index and good calibration. First, we observed that the radiomics signature has a good accuracy to differentiate TNBC and fibroadenoma. Next, we used multivariate logistic regression analysis to construct a combined nomogram. We observed its excellent calibration and attempted to unravel its predictive capacity for differentiating TNBC and fibroadenoma. The nomogram showed a better diagnostic discrimination performance than the Rad-score or clinic model alone, and it can be more intuitive and easily used in distinguishing breast lesions with TNBC and fibroadenoma. Future directions can be associated with the prognostic indicator and treatment schedule and the identification of a risky radiomics signature.

Our present study has several limitations. First, our study was retrospective, and it possessed a potential selection bias. Second, ROIs were drawn manually, and the lack of

Figure 6. Decision curve for the clinical findings, Rad-score, and radiomics nomogram. The gray line represents the assumption that all patients are TNBC cases; the black line refers to the assumption that all patients are fibroadenoma cases. The x-axis denotes the high-risk threshold, and the y-axis indicates the net benefit. The blue, orchid, and light-pink lines represent the clinical model, Rad-score model, and radiomics nomogram, respectively.

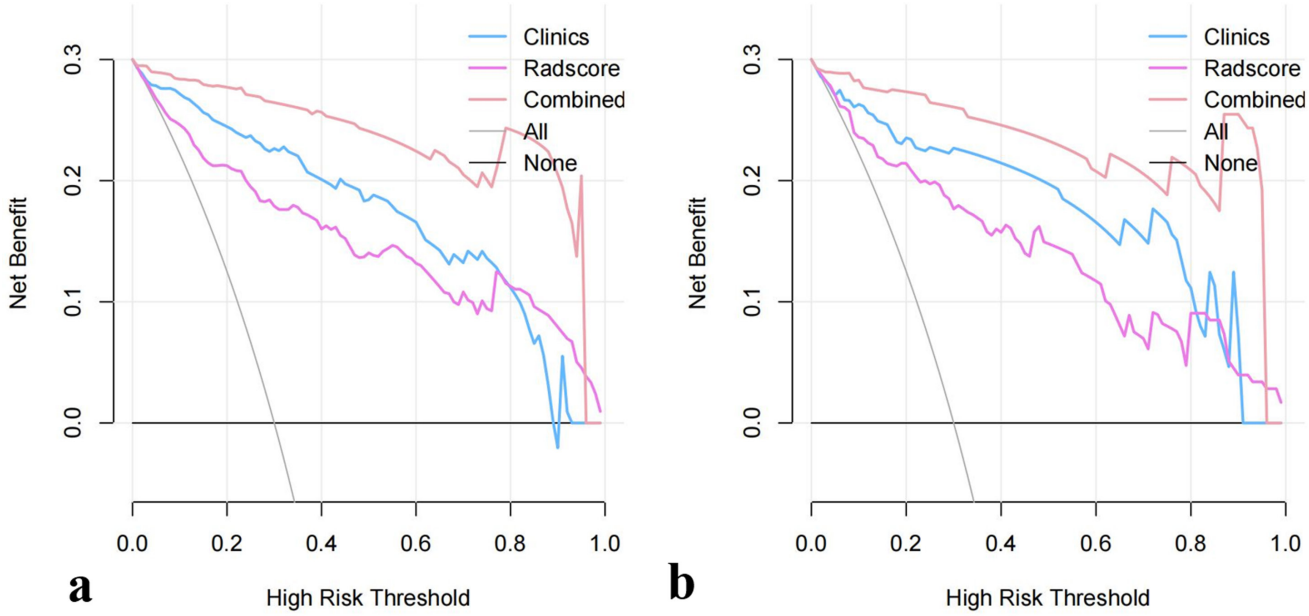

standardization caused by differences in selection can be encountered, although the two radiologists showed excellent interobserver and intro-observer agreement in our study. Fully automatic segmentation tools associated with good diagnostic accuracy should be applied in future studies to avoid such potential faults. Third, the radiomics nomogram may be difficult to generalize because all breast lesions were examined using the same machine and US examination protocol. Further studies are required for multiple types of US and multicenter validation with a larger sample to achieve higher predictive accuracy for clinical application. Fourth, large lesions were not included in this study because of the inability of US to completely present the entire lesion on a single plane.

In conclusion, the present study used US-based images to construct a Rad-score model, which can be an independent biomarker for risk prediction in patients with TNBC. In addition, our study presented a nomogram, with a combination of Rad-score and clinical findings, which exhibited a favorable performance in differentiating TNBC and fibroadenoma. The combined model may possess practicability and value of popularization to reduce the number of biopsies and provide a suitable treatment strategy in the future.

REFERENCES

1. Foulkes WD, Smith IE, Reis-Filho JS. Triple-negative breast cancer. *N Engl J Med* 2010; **363**: 1938–48. https://doi.org/10.1056/NEJMra1001389
2. Siegel RL, Miller KD, Jemal A. Cancer statistics, 2020. *CA Cancer J Clin* 2020; **70**: 7–30. https://doi.org/10.3322/caac.21590
3. Dogan BE, Turnbull LW. Imaging of triple-negative breast cancer. *Ann Oncol* 2012; **23 Suppl 6**: vi23-9. https://doi.org/10.1093/annonc/mds191
4. Yoon GY, Cha JH, Kim HH, Shin HJ, Chae EY, et al. Sonographic features that can be used to differentiate between small triple-negative breast cancer and fibroadenoma. *Ultrasonography* 2018; **37**: 149–56. https://doi.org/10.14366/usg.17036
5. Ko ES, Lee BH, Kim HA, Noh WC, Kim MS, et al. Triple-negative breast cancer: correlation between imaging and pathological findings. *Eur Radiol* 2010; **20**: 1111–17. https://doi.org/10.1007/s00330-009-1656-3
6. Mayerhoefer ME, Materka A, Langs G, Häggström I, Szczypiński P, et al. Introduction to radiomics. *J Nucl Med* 2020; **61**: 488–95. https://doi.org/10.2967/jnumed.118.222893
7. Gillies RJ, Kinahan PE, Hricak H. Radiomics: images are more than pictures, they are data. *Radiology* 2016; **278**: 563–77. https://doi.org/10.1148/radiol.2015151169
8. Zha H-L, Zong M, Liu X-P, Pan J-Z, Wang H, et al. Preoperative ultrasound-based radiomics score can improve the accuracy of the memorial sloan kettering cancer center nomogram for predicting sentinel lymph node metastasis in breast cancer. *Eur J Radiol* 2021; **135**: 109512. https://doi.org/10.1016/j.ejrad.2020.109512
9. Jiang M, Li C-L, Luo X-M, Chuan Z-R, Lv W-Z, et al. Ultrasound-based deep learning radiomics in the assessment of pathological complete response to neoadjuvant chemotherapy in locally advanced breast

cancer. *Eur J Cancer* 2021; **147**: 95–105. https://doi.org/10.1016/j.ejca.2021.01.028
10. Gao Y, Luo Y, Zhao C, Xiao M, Ma L, et al. Nomogram based on radiomics analysis of primary breast cancer ultrasound images: prediction of axillary lymph node tumor burden in patients. *Eur Radiol* 2021; **31**: 928–37. https://doi.org/10.1007/s00330-020-07181-1
11. Luo WQ, Huang QX, Huang XW, Hu HT, Zeng FQ, et al. Predicting breast cancer in breast imaging reporting and data system (bi-rads) ultrasound category 4 or 5 lesions: a nomogram combining radiomics and bi-rads. *Sci Rep* 2019; **9**(1): 11921. https://doi.org/10.1038/s41598-019-48488-4
12. Lambin P, Leijenaar RTH, Deist TM, Peerlings J, de Jong EEC, et al. Radiomics: the bridge between medical imaging and personalized medicine. *Nat Rev Clin Oncol* 2017; **14**: 749–62. https://doi.org/10.1038/nrclinonc.2017.141
13. Lee SE, Han K, Kwak JY, Lee E, Kim E-K. Radiomics of us texture features in differential diagnosis between triple-negative breast cancer and fibroadenoma. *Sci Rep* 2018; **8**(1): 13546. https://doi.org/10.1038/s41598-018-31906-4
14. van Griethuysen JJM, Fedorov A, Parmar C, Hosny A, Aucoin N, et al. Computational radiomics system to decode the radiographic phenotype. *Cancer Res* 2017; **77**: e104–7. https://doi.org/10.1158/0008-5472.CAN-17-0339
15. Ji G-W, Zhu F-P, Zhang Y-D, Liu X-S, Wu F-Y, et al. A radiomics approach to predict lymph node metastasis and clinical outcome of intrahepatic cholangiocarcinoma. *Eur Radiol* 2019; **29**: 3725–35. https://doi.org/10.1007/s00330-019-06142-7
16. Wu Q, Wang S, Chen X, Wang Y, Dong L, et al. Radiomics analysis of magnetic resonance imaging improves diagnostic performance of lymph node metastasis in patients with cervical cancer. *Radiother Oncol* 2019; **138**: 141–48. https://doi.org/10.1016/j.radonc.2019.04.035
17. Traverso A, Wee L, Dekker A, Gillies R. Repeatability and reproducibility of radiomic features: a systematic review. *Int J Radiat Oncol Biol Phys* 2018; **102**: 1143–58. https://doi.org/10.1016/j.ijrobp.2018.05.053
18. Rai R, Holloway LC, Brink C, Field M, Christiansen RL, et al. Multicenter evaluation of mri-based radiomic features: a phantom study. *Med Phys* 2020; **47**: 3054–63. https://doi.org/10.1002/mp.14173
19. Gibbs P, Onishi N, Sadinski M, Gallagher KM, Hughes M, et al. Characterization of sub-1 cm breast lesions using radiomics analysis. *J Magn Reson Imaging* 2019; **50**: 1468–77. https://doi.org/10.1002/jmri.26732
20. Uno H, Cai T, Pencina MJ, D'Agostino RB, Wei LJ. On the c-statistics for evaluating overall adequacy of risk prediction procedures with censored survival data. *Stat Med* 2011; **30**: 1105–17. https://doi.org/10.1002/sim.4154
21. Hu H-T, Wang Z, Huang X-W, Chen S-L, Zheng X, et al. Ultrasound-based radiomics score: a potential biomarker for the prediction of microvascular invasion in hepatocellular carcinoma. *Eur Radiol* 2019; **29**: 2890–2901. https://doi.org/10.1007/s00330-018-5797-0
22. Lambin P, Rios-Velazquez E, Leijenaar R, Carvalho S, van Stiphout RGPM, et al. Radiomics: extracting more information from medical images using advanced feature analysis. *Eur J Cancer* 2012; **48**: 441–46. https://doi.org/10.1016/j.ejca.2011.11.036
23. Conti A, Duggento A, Indovina I, Guerrisi M, Toschi N. Radiomics in breast cancer classification and prediction. *Semin Cancer Biol* 2021; **72**: 238–50. https://doi.org/10.1016/j.semcancer.2020.04.002
24. Gillies RJ, Kinahan PE, Hricak H. Radiomics: images are more than pictures, they are data. *Radiology* 2016; **278**: 563–77. https://doi.org/10.1148/radiol.2015151169
25. Cui X, Zhu H, Huang J. Nomogram for predicting lymph node involvement in triple-negative breast cancer. *Front Oncol* 2020; **10**: 608334. https://doi.org/10.3389/fonc.2020.608334
26. Moon WK, Huang Y-S, Lo C-M, Huang C-S, Bae MS, et al. Computer-aided diagnosis for distinguishing between triple-negative breast cancer and fibroadenomas based on ultrasound texture features. *Med Phys* 2015; **42**: 3024–35. https://doi.org/10.1118/1.4921123
27. Yeo SH, Kim GR, Lee SH, Moon WK. Comparison of ultrasound elastography and color doppler ultrasonography for distinguishing small triple-negative breast cancer from fibroadenoma. *J Ultrasound Med* 2018; **37**: 2135–46. https://doi.org/10.1002/jum.14564
28. Balachandran VP, Gonen M, Smith JJ, DeMatteo RP. Nomograms in oncology: more than meets the eye. *Lancet Oncol* 2015; **16**: e173-80. https://doi.org/10.1016/S1470-2045(14)71116-7
29. Liang W, Yang P, Huang R, Xu L, Wang J, et al. A combined nomogram model to preoperatively predict histologic grade in pancreatic neuroendocrine tumors. *Clin Cancer Res* 2019; **25**: 584–94. https://doi.org/10.1158/1078-0432.CCR-18-1305
30. Cai J, Zheng J, Shen J, Yuan Z, Xie M, et al. A radiomics model for predicting the response to bevacizumab in brain necrosis after radiotherapy. *Clin Cancer Res* 2020; **26**: 5438–47. https://doi.org/10.1158/1078-0432.CCR-20-1264
31. Koh J, Lee E, Han K, Kim S, Kim D-K, et al. Three-dimensional radiomics of triple-negative breast cancer: prediction of systemic recurrence. *Sci Rep* 2020; **10**(1): 2976. https://doi.org/10.1038/s41598-020-59923-2
32. Braman N, Prasanna P, Whitney J, Singh S, Beig N, et al. Association of peritumoral radiomics with tumor biology and pathologic response to preoperative targeted therapy for her2 (erbb2)-positive breast cancer. *JAMA Netw Open* 2019; **2**: e192561. https://doi.org/10.1001/jamanetworkopen.2019.2561